Ex vivo rheology of spider silk

N. Kojić[1,2,*], J. Bico[1,3], C. Clasen[4,5] and G. H. McKinley[1]

[1]*Hatsopoulos Microfluids Laboratory, Department of Mechanical Engineering, MIT and [2]Harvard-MIT Division of Health Sciences and Technology, Cambridge, MA 02139, USA, [3]PMMH-ESPCI, CNRS UMR 7636, 75231 Paris Cedex 05, France, [4]Institut für Technische und Makromolekulare Chemie, 20146 Hamburg, Germany and [5]Departement Chemische Ingenieurstechnieken, Katholieke Universiteit Leuven, 2001 Heverlee, België*

*Author for correspondence (e-mail: kojic@mit.edu)

Summary

We investigate the rheological properties of microliter quantities of the spinning material extracted *ex vivo* from the major ampullate gland of a *Nephila clavipes* spider using two new micro-rheometric devices. A sliding plate micro-rheometer is employed to measure the steady-state shear viscosity of ~1 µl samples of silk dope from individual biological specimens. The steady shear viscosity of the spinning solution is found to be highly shear-thinning, with a power-law index consistent with values expected for liquid crystalline solutions. Calculations show that the viscosity of the fluid decreases 10-fold as it flows through the narrow spinning canals of the spider. By contrast, measurements in a microcapillary extensional rheometer show that the transient extensional viscosity (i.e. the viscoelastic resistance to stretching) of the spinning fluid increases more than 100-fold during the spinning process. Quantifying the properties of native spinning solutions provides new guidance for adjusting the spinning processes of synthetic or genetically engineered silks to match those of the spider.

Key words: silk rheology, *Nephila clavipes*, micro-rheometry, extensional viscosity.

Introduction

Over the past decade, numerous studies have shown that spider dragline silk has a number of unique material properties (Becker et al., 2003; Gosline et al., 1999; Shao and Vollrath, 2002), yet how exactly the spider processes its fiber remains unclear. Recent experiments with recombinant spider silk (Lazaris et al., 2002) and other studies performed with silkworms (Shao and Vollrath, 2002) show that careful control of the processing conditions for fiber spinning is key to obtaining superior mechanical properties in spun silks. Forced silking at different rates results in modified kinematics in the spinning canal and substantial changes in the mechanical properties of the resulting silk fibers (Perez-Rigueiro et al., 2005). A detailed microscopic study of spider silk spinning involving whole spider silk glands suggests that at least two physical processes are important (Knight and Vollrath, 1999): (1) shear-thinning of the silk solution in the ducts that deliver the fluid towards the spinneret (this is, in turn, related to the liquid crystallinity of the protein solution) and (2) pronounced elongation of the long protein chains during the spinning process results in a highly aligned microstructure after the silk dries.

To further understand this complex flow process it is essential to elucidate the rheological properties of the initial liquid spinning material, commonly referred to as 'spinning dope' (Vollrath and Knight, 2001), that is stored in the spinning glands of the spider (Chen et al., 2002). Although the spinning dope is a concentrated aqueous solution containing 25–30 wt% protein, all rheological experiments to date have been performed with diluted solutions (typically <5 wt% of protein) (Chen et al., 2002).

Recently, processing experiments have been performed with reconstituted silk solutions obtained from the silkworm *Bombyx mori* (Jin and Kaplan, 2003). Micellar solutions with ~8 wt% silk were reconstituted using dialysis. However, in order to produce spinnable fibers, a high-molecular-mass linear polymer (polyethylene oxide with molecular mass of 0.9×10^6 g mol^{-1}) was added to the reconstituted solutions. This additional component augments the 'spinnability' of the dope by increasing the extensional or 'tensile' viscosity of the fluid and prevents capillary break-up of the fluid jet. The resulting spun fibers exhibited morphological features, such as increased birefringence and alignment, that are similar to the native silk fiber (Magoshi et al., 1994). The birefringence properties of raw spider silk have also been observed and investigated by Knight and Vollrath (Knight and Vollrath, 1999). These experiments suggest that native silkworm and spider silk solutions possess significant non-Newtonian fluid properties (Chen et al., 2002; Terry et al., 2004), however more insight would be gained through direct rheological

characterization of the native, concentrated spider silk dope. For clarity, we provide in the Appendix a glossary of some of the most important rheological concepts that are essential for understanding the properties of this complex protein solution.

Recently published results (Terry et al., 2004) of bulk shear rheometry on larger scale samples of silkworm silk solutions indicate strong viscoelastic properties for silk dope with a zero-shear-rate viscosity on the order of 10^3 Pa.s and a critical rate of the onset of shear thinning on the order of $1\ s^{-1}$. Phase separation and unstable flow conditions above this critical rate were interpreted as indication for a shear-induced beta-sheet formation.

The volume of spinning dope that can be harvested from a single major ampullate gland of *N. clavipes* is approximately 5–10 μl. Besides the minute quantity available, the dope is viscous (Willcox et al., 1996) and tends to dry with time, making it difficult to obtain reliable viscometric data. Many of these difficulties can be overcome by using micro-rheometry. The majority of micro-rheometric techniques available for the characterization of complex biofluids rely on Brownian forcing of microscopic tracer beads. The rheological properties of the surrounding fluid matrix are obtained from the time-correlated displacement of the bead *via* a deconvolution process (Mukhopadhyay and Granick, 2001; Solomon and Lu, 2001). Such techniques are inherently limited to studies of linear viscoelastic properties of the test fluid at small shearing strains. By contrast, the silk spinning process involves large strains and both shearing and extensional kinematic components (Knight and Vollrath, 1999). These large deformations influence the development of non-equilibrium texture morphologies in the spun silk (Vollrath and Knight, 2001) that lead to observational phenomena such as super-contraction (Vollrath et al., 1996) and shape-memory effects (Emile et al., 2006). In order to address these issues, two new micro-rheometric instruments have been constructed: a flexure-based micro-rheometer (Clasen et al., 2006; Clasen and McKinley, 2004; Gudlavalleti et al., 2005) for steady and oscillatory shearing measurements and a capillary break-up micro-rheometer for extensional rheometry (Bazilevsky et al., 1990; McKinley and Tripathi, 2000).

Here, we describe the application of these instruments in measuring the rheological properties of dragline silk solutions extracted from the major ampullate gland of *Nephila* spiders.

Materials and methods

Both of the experimental devices utilized in the present study have been specifically designed to accommodate the small quantities (~1 μl) of fluid available from a single major ampullate gland of the *Nephila clavipes* L. spider, as shown in Fig. 1. Thus, these micro-rheometric devices enable *ex vivo* testing of the native spinning dope from which the spider spins dragline and web frame fibers (Gosline et al., 1999; Vollrath and Knight, 2001).

Dissections were performed using a standard dissecting microscope, and the ampullate glands were extracted and
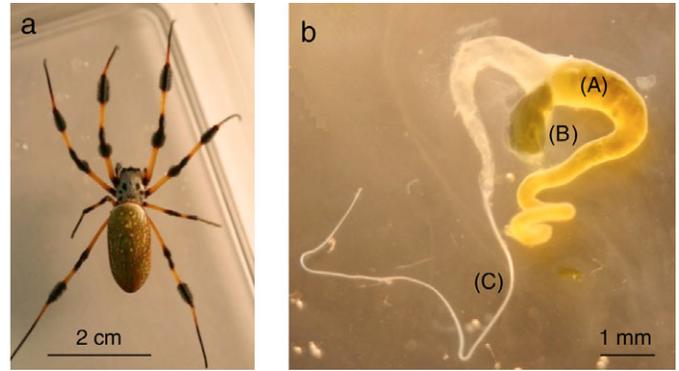

Fig. 1. (a) Adult female *Nephila Clavipes* (golden-orb) spider provided by the Miami Metrozoo, Florida. (b) (A) Dissected major ampullate (MA) gland of the spider. The ~1 μl blob (B) protruding through a rupture of the gland wall near the spinning canal (C) was used for the rheology experiments.

stored under distilled water for less than 5 min whilst being transferred to the micro-rheometers for testing. Each sample was only utilized once due to progressive evaporation of the aqueous phase to the environment.

The flexure-based micro-rheometer generates a plane Couette shearing flow between two plates that are aligned using white light interferometry and separated by a precisely controlled gap of 1–150 μm (Fig. 2a). The plates consist of cylindrical optical flats that are then diamond-machined to provide the required rectangular test surface area. The shear stress exerted on the sample (ranging from 2 to 10^4 Pa) is calculated from the deflection of the upper flexure as the lower one is actuated. The imposed shear rate ($\dot\gamma$), defined as the ratio of the actuated plate velocity (v) and the inter-plate gap (h), $\dot\gamma=v/h$, can be varied over the range $2\times10^{-4}<\dot\gamma<4\times10^2\ s^{-1}$. Further details of the instrumentation are provided elsewhere (Clasen et al., 2006; Clasen and McKinley, 2004).

Recently, it has been noted that the converging flow in the duct of the major ampullate gland has significant extensional kinematics that can lead to pronounced molecular extension and orientation (Knight and Vollrath, 1999; Vollrath and Knight, 2001). If macroscopic volumes of the entangled polymer solution are available, then the extensional viscosity of a viscous liquid can now be measured reliably using filament stretching rheometry (Bhattacharjee et al., 2002). However, given the limited amount of raw dope available, this method becomes impractical. In the present work we have developed a microscale capillary break-up extensional rheometer to measure the transient extensional viscosity η_e (McKinley and Tripathi, 2000). The experimental procedure involves placing a drop of the spinning dope in-between two cylindrical endplates of radius $R_p=1.5$ mm. The plates are then pulled apart to a distance of 5 mm in order to impose a step axial strain on the sample and form a liquid thread (Fig. 3). The instrument can be placed in an environmental chamber to control test temperature and relative humidity if desired; however the present tests were all performed in a standard laboratory
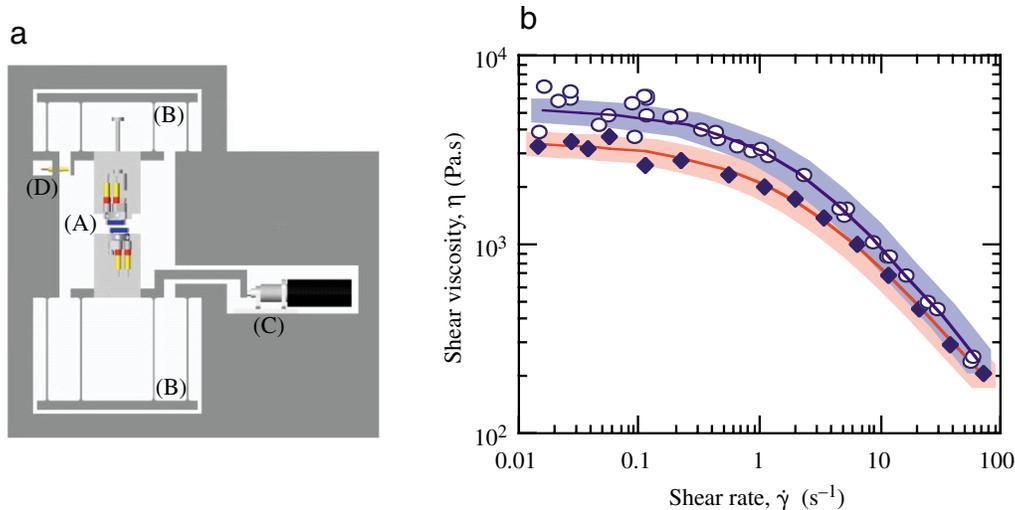
a

b

Fig. 2. (a) Schematic diagram of the flexure-based micro-rheometer. The fluid sample is sheared between two interferometrically aligned flat plates (A). The compound flexure system (B) is actuated by an 'inchworm' motor (C) and provides a planar (Couette) shear flow. The shear stress is deduced from the corresponding deflection of the top fixture as detected by an inductive sensor (D). (b) Shear viscosity of the native silk dope. Diamonds (and shaded red area) correspond to *Nephila clavipes* spider; open circles (and blue shaded area) are from *Bombyx mori* silkworm. The solid lines (blue for silkworm and red for spider) represent the Carreau-Yasuda fit from Eqn 2 to experimental data (markers). Reproducibility was confirmed by testing specimens from two other spiders and silkworms whose abdomens were similar in size. The variation in the data is represented by the shaded band.

environment (T=22°C; relative humidity 25–35%). The viscoelastic fluid column that is formed by the step extensional strain subsequently thins under the action of capillarity, while viscous and elastic forces tend to impede the necking process. The time rate of change of the liquid filament is monitored using a laser micrometer with a resolution of ±10 μm (Omron model ZL4A; Omron, Schaumburg, IL, USA). Gravitational drainage is not important for such small samples, and the filament evolves in a self-similar manner. It has been shown that the apparent extensional viscosity function can be deduced from the self-similar thinning and pinch-off dynamics of the viscous fluid thread (McKinley and Tripathi, 2000) *via* the expression:

$$\eta_e = -0.213 \, [\sigma/(\mathrm{d}R/\mathrm{d}t)] \,. \tag{1}$$

Here, σ is the surface tension of the liquid, $R(t)$ is the midpoint radius of the thread measured with the laser micrometer, and the numerical prefactor is derived from a slender-body lubrication theory for a viscous incompressible Newtonian fluid in order to account for deviations from a purely cylindrical geometry in the vicinity of the endplates (McKinley and Tripathi, 2000).

Due to the high viscosity of the silk and the evaporation of the aqueous solvent, it was not possible to directly measure the surface tension of the silk, and furthermore we are not aware of any published data on this topic. However, we may estimate the range of values to be $30\times10^{-3}{\leqslant}\sigma{\leqslant}60\times10^{-3}$ N m^{-1}. The upper bound is consistent with measured values for other aqueous polymer solutions (Adamson and Gast, 1997; Christanti and Walker, 2001; Cooper-White et al., 2002). The presence of any additional surfactant components in the silk

dope may lower this number to values closer to those of non-water-soluble hydrocarbon-based polymers that are typically of the order of 30×10^{-3} N m^{-1}.

Results

Shear viscosity of ex vivo silk solutions

The sliding plate micro-rheometer was used to measure the shear-rate-dependence of the steady shear viscosity $\eta(\dot{\gamma})$ for a ~1 μl blob of spinning dope extracted from the major ampullate gland. The dope was sheared between two 25 mm^2 optical plates with the gap set to 25 μm (Fig. 2a), and we further assume a no-slip boundary condition between the dope and the optical plates. In the limit of zero shear rate, the data in Fig. 2b show that the viscosity of the spinning dope is η_0=3500 Pa.s (or 3.5×10^6 times the viscosity of water). However, under stronger deformation rates, the dope viscosity drops significantly with increasing shear rate, i.e. the dope has a shear-thinning viscosity (Fig. 2b). This effect is characteristic of concentrated polymer solutions due to the loss of molecular entanglements and can be described by molecular theories or by phenomenological constitutive models such as the Carreau-Yasuda equation (Bird et al., 1987a; Yasuda et al., 1981):

$$\eta = \eta_0 \, [1 + (\dot{\gamma}\lambda)^a]^{(n-1)/a} \,, \tag{2}$$

where λ is a measure of the relaxation time of the viscoelastic fluid (its inverse is the critical shear rate that marks the onset of shear thinning), n is the power-law exponent characterizing the shear-thinning regime observed at high shear rates, and the coefficient a describes the rate of transition between the zero-shear-rate region and the power-law region.
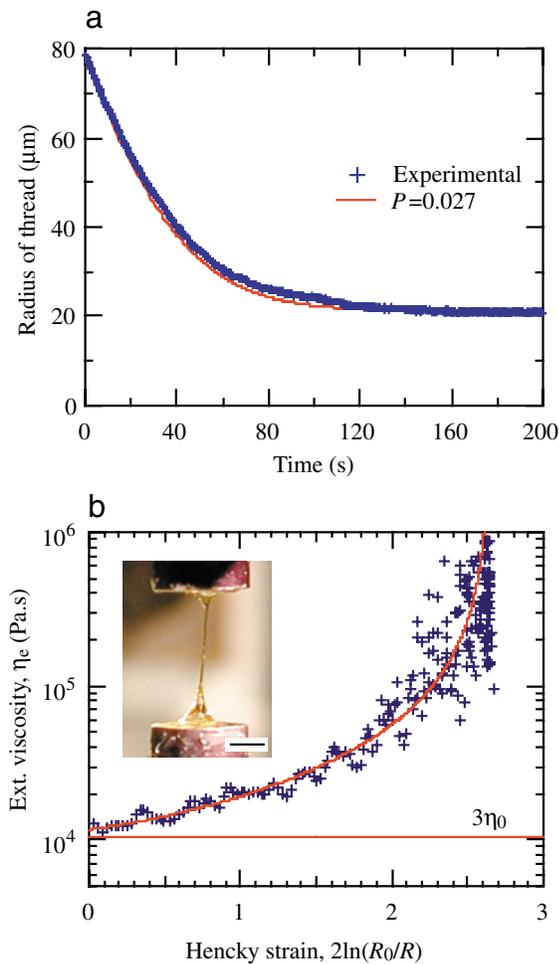
a

b

Fig. 3. (a) Radius R of necking thread formed from the *ex vivo*-obtained *Nephila* dope (measured at thread midpoint, see inset in b) in blue markers. The solid red line represents the model fit using the processability parameter of $P=2.715\times10^{-2}$. (b) The transient extensional rheology of *ex vivo* spider dope. The extensional viscosity is shown as a function of the total strain in the material. Here, R_0 is the initial radius of the thread measured at the midpoint between the plates with a laser micrometer. The decrease of the midpoint radius R was monitored over time (see a). The extensional viscosity was then deduced from Eqn 1 and is represented by the markers. The solid line is an analytical fit of these values. For low strains, we obtain the limit $\eta_e\approx3\eta_0=11\,400$ Pa.s as expected for a Newtonian liquid. Inset, a silk thread of diameter 40 μm formed by separating the plates to a distance of 5 mm and allowing the thread to neck under the action of capillary and viscoelastic stresses (scale bar, 1 mm).

Nonlinear regression of these parameters to our data yields values of $\lambda=0.40$ s, $a=0.68$ and $n=0.18$, which are characteristic for a strongly shear-thinning fluid (Yasuda et al., 1981). We are not aware of any other published data on the *ex vivo* rheology of native *Nephila* dope with which we can compare these values. A comparison to rheological measurements for *B. mori* dope, determined with the same experimental setup and shown in Fig. 2b, gives similar viscoelastic properties for the silk

dopes obtained from the silkworm and the spider. The constitutive parameters obtained with each sample are tabulated in Table 1. The shear-thinning behavior measured in our silkworm dope is consistent with recent experiments performed with a commercial rheometer (Terry et al., 2004), in which the zero-shear-rate viscosity measured was reported to be 'approximately 2 kPa.s' (we measured 5±1 kPa.s). Their measurements also showed that the critical shear-rate above which shear-thinning occurs is of the order 0.5 s^{-1} (we determined 1.7 s^{-1}). No reports of standard error or sample-to-sample variability were reported in this earlier study; the relatively small differences between the two sets of measurements may be due to biological variability as well as to handling of the dope sample.

Extensional rheology

The data in Fig. 3b show that at small strains the extensional viscosity η_e is three times larger than the zero-shear-rate viscosity measured with the shearing micro-rheometer. This observation is consistent with the classical results of Trouton for a Newtonian liquid (Trouton, 1906). However, at large strains, the necking dynamics are greatly retarded as the filament simultaneously strain-hardens and undergoes mass transfer to the surroundings (i.e. evaporative drying). This strain-hardening stabilizes the spinline and leads to the formation of axially uniform filaments (Olagunju, 1999). The apparent extensional viscosity therefore diverges and the thinning fluid thread ultimately dries to become a solid filament with a fixed finite radius. In contrast to an actual dragline filament, which is spun under a constant force corresponding to the weight of a spider (Gosline et al., 1999), in our capillary break-up device there is no externally imposed tension. The final thread radius is measured to be $R_f\approx20$ μm. The solid red line in Fig. 3a corresponds to a one-dimensional model of this drying process, which is discussed in detail below.

Discussion

The strong shear-rate dependence of the silk viscosity shown in Fig. 2 is of considerable importance during extrusion. During a typical spinning process (Shao and Vollrath, 2002; Vollrath and Knight, 2001), the *Nephila* spider draws out a 4 μm-diameter thread at a speed of 20 mm s^{-1} corresponding to a flow rate of $\dot{Q}=0.25$ nl s^{-1}. We approximate the geometry of the long converging spinning canal (or S-duct) shown in Fig. 1b as a truncated cone of length $L=20$ mm and with maximum and minimum diameters of $D=200$ μm and $d=4$ μm, respectively. Although little is known about the actual kinematic boundary conditions at the wall of the spinneret, we assume that there is no-slip between the fluid dope and the wall, as in previous studies (Vollrath and Knight, 2001). For the given geometry and flow rate, the pressure drop associated with steady flow of a viscous shear-thinning dope through the canal can be estimated from hydrodynamic lubrication theory [Bird et al. (Bird et al., 1987a), eq. 4.2-10], which leads to the following expression

for the relative pressure drop for steady flow of a power-law liquid through a linearly tapered tube compared with that expected for a Newtonian fluid:

$$\frac{\Delta P_{\text{silk}}}{\Delta P_{\text{Newtonian}}} = \frac{2^{3(n-1)}\lambda^{n-1}}{4n}\left(\frac{\dot{Q}}{\pi}\right)^{n-1}$$
$$\left[\left(\frac{1}{n}+3\right)\right]^n\left(\frac{d^{-3n}-D^{-3n}}{d^{-3}-D^{-3}}\right). \quad (3)$$

Here, λ and n are obtained from the Carreau-Yasuda model (Eqn 2). This relation is only valid in the shear-thinning regime when the shear rate is larger than the critical shear rate $(1/\lambda)$ and the viscosity is thus well approximated by $\eta(\dot{\gamma})\approx\eta_0(\lambda\dot{\gamma})^{n-1}$. For our truncated cone geometry, the minimum value of the wall shear rate is $\dot{\gamma}=32\dot{Q}/\pi D^3=0.3^{-1}$, which justifies the use of the power law fluid and Eqn 2 and 3 as approximations. The pressure drop required for the shear-thinning silk dope is a factor of 500 lower than that associated with a corresponding viscous Newtonian fluid. Thus, shear-thinning of the liquid crystalline solution reduces the absolute value of the pressure drop in the spinning canal required to sustain flow rates of the order of nanoliters per second.

The pressure drop ΔP_{silk} necessary to push the silk dope through the spinneret at the typical flow rate of $\dot{Q}=0.25$ nl s^{-1} is approximately 4×10^7 Pa. The corresponding energy dissipation rate $\Delta P_{\text{silk}}\dot{Q}\sim10$ μW (due to viscous flow of the silk dope) is comparable to the release rate of potential energy, $MgV_{\text{spin}}\sim20$μW, for a spider descending on a dragline, where M is the mass of the spider (~0.1 g), g is the gravitational constant, and $V_{\text{spin}}=20$ mm s^{-1} is a typical silking speed. By contrast, if the silk dope did not exhibit this pronounced shear-thinning behavior (which is associated with its liquid crystallinity), the viscous dissipation rate required to sustain the corresponding flow rate of a Newtonian fluid would be 5000 μW and hence would significantly exceed the potential energy release rate. Additional sources of energy input would have to be provided by the spider or, conversely, a much lower natural spinning speed would be selected.

This shear-thinning property of the silk dope may also act in conjunction with other proposed mechanisms that facilitate the spinning of the thread, such as a shear-induced transition to a liquid crystalline phase (Vollrath and Knight, 2001), localised slip of the polymer solution on the tube wall (Migler et al., 1993), or a subtle form of lubrication, such as a watery surfactant layer (Vollrath and Knight, 2001) or an analogue to the sericin coat surrounding fibroin fibers spun by *B. mori* (Kaplan et al., 1994).

In contrast to the observations of shear-thinning, the measurements of the transient extensional rheology in the micro-capillary break-up extensional rheometer (or μCABER) show that in an elongational flow the material's resistance to stretching increases with elapsed time (and imposed strain). The importance of this strain-hardening phenomena for the spinning of dragline silk appears to have been first noted by Ferguson and Walters (Ferguson and Walters, 1988) and

prevents the capillary break-up of an elongating viscoelastic fluid filament (Olagunju, 1999).

In addition to being sheared, the proteins in the spinning dope are also stretched due to the elongational flow experienced in the converging duct and the subsequent spinline. An extensional flow of this type is characterized by the deformation rate and the total Hencky strain accumulated, which can be defined in the present problem as $\epsilon=2\ln(D/d)\approx8$ (Bird et al., 1987a). This large value of the extensional strain suggests that the spidroin molecules are being considerably extended (Perkins et al., 1997). This extension thus plays a key role in the molecular alignment necessary for the exceptional mechanical properties of the spun fiber. The characteristic strain rate for this elongational flow is given by:

$$\dot{\epsilon} = \frac{4\dot{Q}}{\pi L}\left(\frac{1}{d^2}-\frac{1}{D^2}\right) = 1\,\text{s}^{-1}. \quad (4)$$

This rate of stretching can be compared with the liquid relaxation time *via* the Deborah number [see Appendix as well as Bird et al. (Bird et al., 1987a)], defined as $De=\lambda\dot{\epsilon}$, which provides a dimensionless measure of the importance of viscoelastic properties. The computed value of $De\approx0.5$ indicates that viscoelastic effects should result in modest strain hardening of the dope (i.e. an increase in the resistance to stretching with increasing strain) (Bird et al., 1987a). This strain-hardening effect is due to chain-stretching of the entangled spidroin macromolecules, and the presence of this additional elastic stress can be evaluated from the extensional viscosity of the liquid.

The time evolution in the neck radius that is depicted in Fig. 3a is driven by the capillary pressure and resisted by the viscoelastic stresses in the elongating fluid thread. The necking rate is further modulated by evaporation of solvent (water) from the thread. This evaporation rate becomes larger as time proceeds due to the increasing surface area-to-volume ratio. The loss of water also results in an increase in the fluid viscosity and a further slow-down in the rate of necking. A simple model that captures the essential physics of this filament thinning/drying process through a time-dependent viscosity function is given by Tripathi et al. (Tripathi et al., 2000). In this analysis, a 'lumped parameter' model is developed that describes the rate of mass transfer in terms of a single dimensionless group referred to as a processability parameter, P. This parameter is defined as the ratio of the two relevant time scales in the problem: the time scale for capillary thinning and the time scale for diffusion of water through the viscous protein dope to the free surface. The characteristic time for capillary thinning is $t_{\text{cap}}\sim\eta_0 R_0/\sigma$ (for a viscous fluid) and the time scale for diffusion [which in our case limits water removal from the thread (Kojic et al., 2004)] is $t_{\text{diff}}\sim R_0^2/D_{\text{w}}$, where R_0 and D_{w} are the initial thread radius and the diffusivity of water through the dope, respectively. We have recently reported a value of $D_{\text{w}}=2\times10^{-5}$ mm^2 s^{-1} for the diffusivity of water through the *Nephila* spinning dope (Kojic et al., 2004). Using this value, along with an initial radius of $R_0=78$ μm (see

Fig. 3a) and the expected range $30\times10^{-3}\leqslant\sigma\leqslant60\times10^{-3}$ N m^{-1} for the surface tension, we obtain the following estimate of the processability parameter:

$$1.6\times10^{-2} \leqslant P \approx \frac{D_{\mathrm{w}}\eta_0}{R_0\sigma} \leqslant 3.2\times10^{-2}\ . \qquad (5)$$

The analysis of Tripathi et al. (Tripathi et al., 2000) utilizes the parameter P to yield a time-varying fluid viscosity given by:

$$\eta(t) = \eta_0\exp\left(2P\int_0^t \frac{R_0}{R(t)}\ \mathrm{d}t\right)\ . \qquad (6)$$

Combining this time-dependent viscosity with Eqn 1 results in an integro-differential equation for calculating the evolution of the radius of the thinning thread.

Alternatively, it is possible to apply this theory directly to the present microcapillary break-up measurements treating P as an arbitrary fitting parameter. The results of using a best-fit value of $P=2.715\times10^{-2}$ are shown in Fig. 3a by the solid red line. This best fit value of the processability parameter is in good agreement with the *a priori* estimate given above.

The resistance of the fluid thread to further stretching is characterized by the apparent extensional viscosity (derived from Eqns 1, 6) as presented in Fig. 3b over the entire course of the filament evolution. At large strains, the filament undergoes strain-hardening due to the combined action of molecular elongation and solvent evaporation and ultimately becomes a solid thread with a constant diameter. The extensional viscosity increases by 100-fold during the capillary thinning of the filament radius. This strain-hardening plays an important role in the fiber spinning process by inhibiting capillary thread break-up and stabilizing the spinline.

Conclusions

In this work, we have used two new micro-rheometric devices that utilize less than 5 μl of fluid for a test and enable the measurement of the steady and transient rheological properties of *ex vivo* samples of biopolymer solutions such as spider and silkworm spinning dope. The devices are able to impose large deformation rates and large strains that match the range of deformations experienced *in vivo*. Our measurements show that the steady shear viscosities $\eta(\dot{\gamma})$ of *N. clavipes* and *B. mori* spinning solutions have very large zero-shear-rate viscosities but shear-thin dramatically above a critical deformation rate (see Table 1). By contrast, in extensional flow, the apparent extensional viscosity of the spider silk dope increases without limits due to the combined action of molecular elongation and solvent evaporation.

Orb-weaving spiders use a specialized fiber-spinning process that exploits the nonlinear rheology of a complex fluid. In the spinning canal of *N. clavipes*, the shear viscosity of the spinning dope decreases by an order of magnitude and thus reduces the pressure-drop along the canal, whereas the extensional viscosity increases by a factor of 100 to stabilise the fluid thread and inhibit capillary break-up of the spun thread. Tailoring the rheological properties of artificial spinning dopes containing genetically modified or reconstituted silks to match the *ex vivo* properties of the natural dope may prove essential in enabling us to successfully process novel synthetic materials with mechanical properties comparable to, or better than, those of natural spider silk.

Table 1. *Constitutive parameters for the shear viscosity of B. mori and N. clavipes spinning dope*

	η_0 (Pa.s)	λ (s)	n	a
Bombyx mori	5200	0.57	0.17	0.80
Nephila clavipes	3500	0.40	0.18	0.68

η_0, zero shear viscosity; λ, relaxation time; n, power-law index; a, transition parameter of the Carreau-Yasuda equation (Eqn 2).

Appendix/glossary

In this glossary we provide brief working definitions for some of the most important rheological concepts utilized in this work and provide references to other primary sources for additional reading.

Constitutive equation

Also often described as a 'rheological equation of state'. Such equations relate the tensorial state of stress in a complex fluid to the entire deformation history imposed on it. If the relationship between an imposed shear-rate and the resulting shear stress is nonlinear then the fluid is 'non-Newtonian'. Constitutive equations may be constructed empirically or derived from molecular-based kinetic theories (Bird et al., 1987a; Bird et al., 1987b).

Shear-thinning viscosity

One of the most common rheological features of complex fluids is a nonlinear relationship between the shear stress (τ) and the shear rate ($\dot{\gamma}$). For most polymeric systems the steady shear viscosity (defined as the ratio of the measured shear stress to the imposed shear rate at steady state; $\eta\equiv\tau/\dot{\gamma}$) decreases as the deformation rate increases due to increasing flow-alignment of the underlying microstructure. The process is particularly dramatic and leads to a very pronounced decrease in the viscosity and increasing optical anisotropy for liquid crystalline polymers (Burghardt, 1998). This effect is known generically as 'shear-thinning' and is demonstrated in Fig. 2. In the limit of low shear rates, the relationship between stress and rate reduces to a simple linear one (i.e. the fluid approaches the limit of a simple Newtonian fluid) and the steady shear viscosity approaches a constant value that is defined as the zero-shear-rate viscosity; $\lim \eta(\dot{\gamma})\rightarrow\eta_0$ as $\dot{\gamma}\rightarrow0$. The Carreau-Yasuda model presented in the text is a relatively simple example of a constitutive model that can describe this transition from Newtonian to shear-thinning. The model is derived by considering the rate of creation and destruction of molecular entanglements in a concentrated polymer solution or melt.

Numerous other constitutive equations (for example, the Giesekus model or the Phan-Thien–Tanner model) can also capture the general trends shown by our data; however, in many cases, these equations contain additional model parameters that can only be determined from a more extensive range of rheological tests. The texts by Bird et al. (Bird et al., 1987a; Bird et al., 1987b) compare and contrast the relative benefits of these different constitutive models.

Liquid crystalline solutions

Liquid crystalline solutions are distinguished by the rigidity and local ordering of the constituent molecules (in contrast to the random walk conformation associated with flexible macromolecules). This local molecular ordering can lead to phase transitions as the concentration is increased or the system temperature is reduced. In addition, the coupling between imposed mechanical deformations and molecular ordering leads to optical anisotropy in the solutions that is manifested in effects such as flow-induced birefringence (Burghardt, 1998). Such effects have been measured in protein solutions obtained from silkworms and from spiders (Magoshi et al., 1994; Willcox et al., 1996) and are discussed in detail in the review of Vollrath and Knight (Vollrath and Knight, 2001).

Extensional viscosity

The extensional viscosity of a fluid is a measure of the resistance to elongational (stretching) deformations and is defined as a ratio of the measured tensile stress difference to the imposed rate of stretching. Although perhaps this concept is initially puzzling to contemplate, some physical understanding may be attained by recognizing that the extensional viscosity holds the same relationship to the shear viscosity of a fluid as the Young's modulus (E) does to the shear modulus (G) for an elastic solid. Indeed, for an incompressible Newtonian fluid, the extensional viscosity is precisely three times the shear viscosity, a result first obtained by Trouton 100 years ago (Trouton, 1906), just as the Young's modulus is three times the shear modulus for an incompressible Hookean solid. For non-Newtonian fluids such as polymer solutions, the extensional viscosity is an independent material function that cannot be determined from the shear viscosity. Typically, the extensional viscosity of a complex fluid is a function of both the rate of elongation and the total strain imposed and this governs the 'spinnability' of a fluid thread (Macosko, 1994).

Strain-hardening

For many polymeric systems it is found that the extensional viscosity increases with the total strain imposed on the system. This is a consequence of the increasing molecular elongation of the flexible polymer chains as the external strain is increased and is referred to as strain-hardening or sometimes 'strain-stiffening' (Nguyen and Kausch, 1999). This increase in the extensional viscosity is only to be expected if the rate of deformation imposed on the fluid is sufficiently rapid to exceed local relaxation of the chain back towards equilibrium; this criterion is parameterized by the Deborah number of the flow.

The Deborah number

The Deborah number provides a dimensionless measure of how important non-Newtonian effects are expected to be in a given deformation. The Deborah number represents a ratio of the intrinsic relaxation time of the polymeric liquid to the characteristic flow time scale (or equivalently the product of relaxation time with the rate of deformation) of a particular flow process (McKinley, 2005). For example, if a polymer chain can relax back to its equilibrium configuration (through Brownian motion) faster than it is deformed ($De<1$) then the material will not show strain-hardening in elongation, or shear-thinning in steady shear flow and will instead flow in the same manner as a viscous Newtonian fluid.

References

Adamson, A. W. and Gast, A. P. (1997). *Physical Chemistry of Surfaces* (6th edn). New York: Wiley-Interscience.

Bazilevsky, A. V., Entov, V. M. and Rozhkov, A. N. (1990). Liquid filament microrheometer and some of its applications. In *Third European Rheology Conference* (ed. D. R. Oliver), pp. 41-43. Amsterdam: Elsevier Applied Science.

Becker, N., Oroudjev, E., Mutz, S., Cleveland, J. P., Hansma, P. K., Hayashi, C. Y., Makarov, D. E. and Hansma, H. G. (2003). Molecular nanosprings in spider capture-silk threads. *Nat. Mat.* **2**, 278-283.

Bhattacharjee, P. K., Oberhauser, J. P., McKinley, G. H., Leal, L. G. and Sridhar, T. (2002). Extensional rheometry of entangled solutions. *Macromolecules* **25**, 10131-10148.

Bird, R. B., Armstrong, R. C. and Hassager, O. (1987a). *Dynamics of Polymeric Liquids, Volume 1, Fluid Mechanics*. New York: Wiley Interscience.

Bird, R. B., Curtiss, C. F., Armstrong, R. C. and Hassager, O. (1987b). *Dynamics of Polymeric Liquids, Volume 2, Kinetic Theory*. New York: Wiley Interscience.

Burghardt, W. R. (1998). Molecular orientation and rheology in sheared lyotropic liquid crystalline polymers. *Macromol. Chem. Phys.* **199**, 471-488.

Chen, X., Knight, D. P. and Vollrath, F. (2002). Rheological characterization of nephila spidroin solution. *Biomacromolecules* **3**, 644-648.

Christanti, Y. and Walker, L. M. (2001). Surface tension driven jet break up of strain hardening polymer solutions. *J. Non-Newtonian Fluid Mech.* **100**, 9-26.

Clasen, C. and McKinley, G. H. (2004). Gap-dependent microrheometry of complex liquids. *J. Non-Newtonian Fluid Mech.* **124**, 1-10.

Clasen, C., Gearing, B. and McKinley, G. H. (2006). Microrheology – the flexure-based microgap rheometer (FMR). *J. Rheol.* In press.

Cooper-White, J. J., Fagan, J. E., Tirtaatmadja, V., Lester, D. R. and Boger, D. V. (2002). Drop formation dynamics of constant low-viscosity, elastic fluids. *J. Non-Newtonian Fluid Mech.* **106**, 29-59.

Emile, O., Le Floch, A. and Vollrath, F. (2006). Biopolymers: shape memory in spider draglines. *Nature* **440**, 621.

Ferguson, J. and Walters, K. (1988). Of spiders and spinning. *Chem. Britain* **1988**, 39-42.

Gosline, J. M., Guerette, P. A., Ortlepp, C. S. and Savage, K. N. (1999). The mechanical design of spider silks: from fibroin sequence to mechanical function. *J. Exp. Biol.* **202**, 3295-3303.

Gudlavalleti, S., Gearing, B. and Anand, L. (2005). Flexure-based micromechanical testing machines. *Exp. Mech.* **45**, 412-419.

Jin, H. J. and Kaplan, D. L. (2003). Mechanism of silk processing in insects and spiders. *Nature* **424**, 1057-1061.

Kaplan, D., Adams, W. W., Farmer, B. and Viney, C. (1994). *Silk Polymers: Materials Science and Biotechnology*. Washington DC: ACS.

Knight, D. P. and Vollrath, F. (1999). Liquid crystals and flow elongation in a spider's silk production line. *Proc. R. Soc. Lond. B Biol. Sci.* **266**, 519-523.

Kojic, N., Kojic, M., Gudlavalleti, S. and McKinley, G. H. (2004). Solvent removal during synthetic and nephila fiber spinning. *Biomacromolecules* **5**, 1698-1707.

Lazaris, A., Arcidiacono, S., Huang, Y., Zhou, J. F., Duguay, F., Chretien, N., Welsh, E. A., Soares, J. W. and Karatzas, C. N. (2002). Spider silk fibers spun from soluble recombinant silk produced in mammalian cells. *Science* **295**, 472-476.

Macosko, C. (1994). *Rheology: Principles, Measurements and Applications*. New York: Wiley-VCH.

Magoshi, J., Magoshi, Y. and Nakamura, S. (1994). Mechanism of fiber formation of silkworm. *Silk Polymers* **544**, 292-310.

McKinley, G. H. (2005). Dimensionless groups for understanding free surface flows of complex fluids. *Soc. Rheol. Bull.* **2005**, 6-9.

McKinley, G. H. and Tripathi, A. (2000). How to extract the Newtonian viscosity from capillary breakup measurements in a filament rheometer. *J. Rheol.* **44**, 653-671.

Migler, K. B., Hervet, H. and Leger, L. (1993). Slip transition of a polymer melt under shear stress. *Phys. Rev. Lett.* **70**, 287-290.

Mukhopadhyay, A. and Granick, S. L. (2001). Micro and nanorheology. *Curr. Opin. Colloid Interface Sci.* **6**, 423-429.

Nguyen, T. Q. and Kausch, H.-H. (1999). *Flexible Polymer Chains in Elongational Flow: Theory and Experiment*. Berlin: Springer-Verlag.

Olagunju, D. O. (1999). A 1-D theory for extensional deformation of a viscoelastic filament under exponential stretching. *J. Non-Newtonian Fluid Mech.* **87**, 27-46.

Perez-Rigueiro, J., Elices, M., Plaza, J., Real, J. I. and Guinea, G. V. (2005). The effect of spinning forces on spider silk properties. *J. Exp. Biol.* **208**, 2633-2639.

Perkins, T. T., Smith, D. E. and Chu, S. (1997). Single polymer dynamics in an elongational flow. *Science* **276**, 2016-2021.

Shao, Z. and Vollrath, F. (2002). Surprising strength of silkworm silk. *Nature* **418**, 741.

Solomon, M. and Lu, Q. (2001). Rheology and dynamics of particles in viscoelastic media. *Curr. Opin. Colloid Interface Sci.* **6**, 430-437.

Terry, A. E., Knight, D. P., Porter, D. and Vollrath, F. (2004). pH induced changes in the rheology of silk fibroin solution from the middle division of Bombyx mori silkworm. *Biomacromolecules* **5**, 768-772.

Tripathi, A., Whittingstall, P. and McKinley, G. H. (2000). Using filament stretching rheometry to predict strand formation and "processability" in adhesives and other non-Newtonian fluids. *Rheol. Acta* **39**, 321-337.

Trouton, F. T. (1906). On the coefficient of viscous traction and its relation to that of viscosity. *Proc. R. Soc. Lond. A* **77**, 426-440.

Vollrath, F. and Knight, D. P. (2001). Liquid crystalline spinning of spider silk. *Nature* **410**, 541-548.

Vollrath, F., Holtet, T., Thogersen, H. C. and Frische, S. (1996). Structural organization of spider silk. *Proc. R. Soc. Lond. B Biol. Sci.* **263**, 147-151.

Willcox, P. J., Gido, S. P., Muller, W. and Kaplan, D. L. (1996). Evidence of a cholesteric liquid crystalline phase in natural silk-spinning processes. *Macromolecules* **29**, 5106-5110.

Yasuda, K., Armstrong, R. C. and Cohen, R. E. (1981). Shear-flow properties of concentrated-solutions of linear and star branched polystyrenes. *Rheol. Acta* **20**, 163-178.